Competition between Charge-Transfer Exciton Dissociation and Direct Photocarrier Generation in Molecular Donor-Acceptor Compounds

Jun'ya Tsutsumi (堤潤也),[1] Toshikazu Yamada (山田寿一),[1] Hiroyuki Matsui (松井弘之),[1,2] Simon Haas,[1] and Tatsuo Hasegawa (長谷川達生)[1,*]

[1]*Photonics Research Institute (PRI), National Institute of Advanced Industrial Science and Technology (AIST), Tsukuba, Japan*
[2]*Department of Advanced Materials Science, The University of Tokyo, Kashiwa, Japan*

(Received 22 September 2010; published 24 November 2010)

The interfacial charge-separation and photovoltaic characteristics of a molecular donor-acceptor charge-transfer compound were examined. Measurements of laser beam-induced currents on the single crystals allowed selective detection of hole and electron photocurrents through the metal–semiconductor interfaces. This method also reveals the exceptionally long diffusion length of 20 μm in the crystal. The transition from charge-transfer exciton dissociation to direct photocarrier generation is discussed on the basis of the photon-energy-dependent diffusion length and photon-to-current conversion spectrum.

DOI: 10.1103/PhysRevLett.105.226601 PACS numbers: 72.40.+w, 71.35.−y, 72.80.Le

The creation of excitons is the initial and most fundamental step in photocurrent generation in organic photovoltaic cells (OPCs) [1]. This feature is closely associated with fairly strong excitonic effects in both small-molecule and polymeric organic semiconductors [1–3]. These effects originate from the weak van der Waals intermolecular interactions and the low-dimensional nature of the electronic states, in addition to the low dielectric constant of the materials. As a result, OPCs are now occasionally referred as ''excitonic solar cells'' [4,5]. For example, the operation of small-molecule-based OPCs is based on the creation of Frenkel excitons whose electronic excitations are confined exclusively to the individual molecular units. This strongly localized nature leads to the ready quenching of excitons before they can form a geminate electron-hole pair and to the limitation of the active photon-energy range for excitonic absorption to above about 1.7 eV [6–9]. It has been suggested that these disadvantages are the main challenges in terms of the further improvement of OPCs [10–14]. In contrast, another type of optically excited state known as the charge-transfer (CT) exciton state exists in organic semiconductors. The CT exciton becomes the lowest electronic excitation state in donor-acceptor combinations where the oscillator strength is very high, leading to efficient excitation [15]. The use of such donor-acceptor CT excitons should permit the tuning of the optical gap energy in the range between 0.5 and 2 eV, depending on the donor-acceptor combination [16].

In this Letter, we report the fundamental charge-dissociation processes of CT excitons for photoelectric conversion. For this purpose, we selected single crystals of a typical donor-acceptor CT complex of dibenzotetrathiafulvalene (DBTTF) with tetracyanoquinodimethane (TCNQ) [Fig. 1(a)], which has an optical gap energy of 0.7 eV and is stable under atmospheric conditions [17,18]. We investigated the interfacial charge-separation and diffusion characteristics of the CT excitons and photogenerated charge carriers in the single crystal by using the high-spatial-resolution laser beam-induced current (LBIC) technique. From the results of this study, we successfully fabricated a metal–insulator–metal (MIM)-type photovoltaic (PV) diode. We discuss the contribution of CT excitons and directly generated photocarriers to the PV characteristics of this device.

High-quality single crystals of DBTTF-TCNQ, with shiny as-grown $0\bar{1}1$ crystal surfaces and a typical size of $0.8 \times 0.2 \times 0.2$ mm^3, were obtained by the physical vapor-transport technique [19] under a N_2 gas flow of 20 mL min^{-1}. Anodes and cathodes were then fabricated on top of the single crystal surfaces by vacuum deposition of films of Au or an organic metal, such as the CT compound of tetrathiafulvalene (TTF) with TCNQ. For high-spatial-resolution measurements by LBIC [20,21], we used a continuous-wave He-Ne laser ($h\nu = 2.0$ eV) or semiconductor lasers with various emission energies ($h\nu = 0.9$, 1.3, 1.5, 2.0, 2.4, or 3.1 eV). The laser light was chopped and finely focused cylindrically on top of the single crystal, and the illuminated position was scanned along the crystal long axis, as shown schematically in Fig. 1(b). The short-circuit photocurrent I_{sc} was then detected by a lock-in technique as a function of the position of illumination. We did not observe any phase delay in the LBIC response at the frequency range from 2 to 300 Hz, so we used the chopping frequency of 25 Hz for all the LBIC measurements. The measurements were typically performed in vacuum with a laser spot size of 2×30 μm^2, a light intensity of 100 mW cm^{-2}, and a scan speed of 10 μm min^{-1}.

The results of typical LBIC measurements on a DBTTF-TCNQ single crystal with a pair of Au electrodes are shown in Fig. 1(c). These results were obtained by using the He-Ne laser as the source of illumination. In the figure, the origin of the abscissa is set at the metal–semiconductor interface on the left. A photocurrent was detected both at

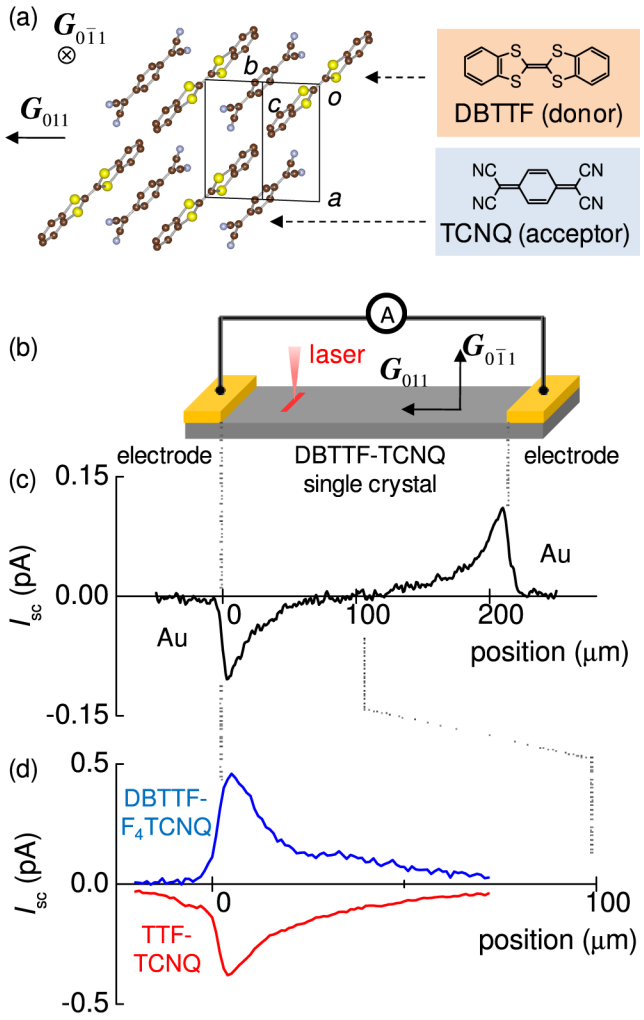

FIG. 1 (color online). (a) Molecular and crystal structure of DBTTF-TCNQ. (b) Scheme for LBIC measurement. (c) Photocurrent profile for the DBTTF-TCNQ single crystal with Au electrodes and (d) with TTF-TCNQ and DBTTF-F_4TCNQ electrodes.

the left- and right-hand metal–semiconductor interfaces. The photocurrent response with centrosymmetric features was observed, with negative and positive signs at the left- and right-hand interfaces, respectively. The photocurrent curves shown in Fig. 1(c) also exhibit a very gradual decay in the surface region of the semiconductor. The decay length is exceptionally long, reaching around 20 μm.

In Fig. 1(d), we present the LBIC profiles for devices with films of TTF-TCNQ and DBTTF-F_4TCNQ (F_4TCNQ = tetrafluorotetracyanoquinodimethane) as electrodes. The sign of the photocurrent depended on the kind of electrode material, providing clear evidence regarding the balance between hole and electron conduction through the metal–semiconductor interfaces. The positive photocurrent observed with DBTTF-F_4TCNQ corresponds to efficient hole conduction, indicating the matching between the electrode Fermi level and semiconductor valence band. In contrast, the negative photocurrent observed with TTF-TCNQ corresponds to efficient electron conduction, indicating the matching between the electrode Fermi level and semiconductor conduction band. The current amplitudes were higher than those obtained with Au, implying a higher efficiency of interfacial charge separation. These results are fairly consistent with n- and p-type operation as observed in DBTTF-TCNQ-based field-effect transistors with TTF-TCNQ and DBTTF-F_4TCNQ films as source or drain electrodes, respectively [22].

On the basis of these results, we fabricated a MIM-type single-crystalline PV diode, as shown in the inset in Fig. 2(a). The device was fabricated with asymmetrically configured metal electrodes consisting of a DBTTF-F_4TCNQ film as the anode and a TTF-TCNQ film as the cathode. As a result of the respective hole- and electron-ejecting natures of these materials, positive photocurrents were integrated at both the

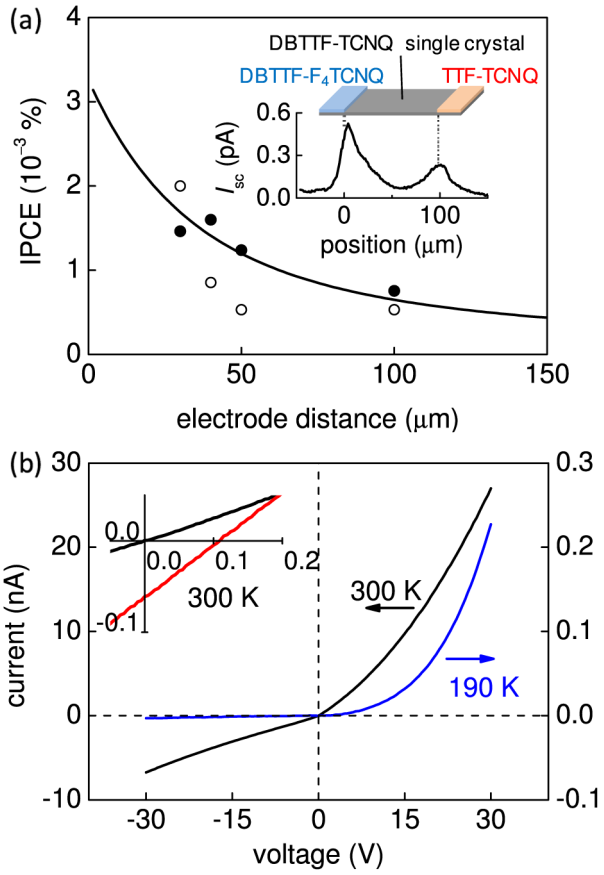

FIG. 2 (color online). (a) Dependence of IPCE (at $h\nu$ = 2.0 eV) on the electrode distance of MIM-type PV diodes, where the filled circles are obtained from the LBIC profiles, whereas the open circles are obtained by illumination over the whole areas of the devices. The solid line is a simulation curve based on a one-dimensional diffusion model. The inset shows an LBIC profile observed for a MIM-type PV diode composed of a DBTTF-TCNQ single crystal with TTF-TCNQ as the cathode and DBTTF-F_4TCNQ as the anode. (b) Current-voltage characteristics measured in the dark for the MIM-type PV diode at 300 and 190 K. The inset shows the current-voltage characteristics at 300 K in the presence (red line) and absence (black line) of illumination (AM1.5, simulated solar illumination with air mass 1.5 filter).

metal–semiconductor interfaces. The dependence of the incident photon-to-current conversion efficiency (IPCE, Φ) on the electrode distance is shown in Fig. 2(a). The resulting IPCE data were roughly reproduced by the solid line predicted by the one-dimensional diffusion model $\phi \propto \{1 - \exp(-d/L)\}L/d$, where L is the decay length of 20 μm. The deviation from the diffusion model should be due to the surface nonuniformity of the single crystals such as defects or strains formed during the crystal growth. The agreement with the one-dimensional diffusion model shows that efficient collection of photogenerated charge carriers (or CT excitons) is possible over a long semiconducting region as a result of the long diffusion lengths. The current-voltage characteristics of the device are shown in Fig. 2(b). The dark current shows noticeable nonlinear and rectifying features, in which the rectification ratio reaches around 10^2 at 190 K. The open-circuit voltage V_{oc} was estimated to be 0.11 V at room temperature and 0.18 V at 210 K in the presence of illumination; this value is comparable to the maximum V_{oc} of 0.3 V estimated from the difference in Fermi levels between TTF-TCNQ and DBTTF-F_4TCNQ [22]. Note that the I_{sc} and fill factor are quite low because of the lateral (or planar) device structure with a long interelectrode distance ($\sim$ 100 μm), which gives a small potential gradient ($\sim$ 1 kV m^{-1}) and a high series resistance between the electrodes.

Figure 3(a) shows the IPCE spectrum for the single-crystalline PV diode recorded under reverse biased conditions at 2 MV m^{-1}. This bias value was chosen so as to afford a similar strength of internal electric field to that present in stack-type OPCs. A photocurrent response was clearly observable in the infrared-photon-energy region below 1 eV, and it then gradually increased with the increasing photon energy until it reached about 1.7% at 2 eV. The onset energy (0.8 eV) almost coincided with the edge of the CT exciton absorption (0.7 eV), which provides clear evidence of the existence of a PV effect associated with CT excitons. When the IPCE curve is redrawn as a plot of $(\mathrm{IPCE})^{0.4}$ against $h\nu$, as shown in the inset in Fig. 3(a), a linear dependence can be identified around the threshold region ($h\nu$ = 1.0–1.6 eV). Such a dependence implies an Onsager-type dissociation of the CT exciton into a free electron and a hole, in which the probability of dissociation is determined by the efficiency of thermal dissociation of the bound electron-hole pair [23].

It is evident that the exceptionally long decay length of as much as 20 μm that was observed in the LBIC measurements has a crucial role in the observed PV characteristics. The decay length is considerably longer than that expected for a Frenkel exciton, the value of which has been reported to be a few tens of nanometers [1]. This implies that the diffusion and dissociation characteristic of CT excitons are markedly different from those of Frenkel excitons. To investigate the origin of the exceptionally long decay length, we measured the LBIC profiles for a single crystal of DBTTF-TCNQ at various incident photon energies, and the results of this study are shown in Fig. 4.

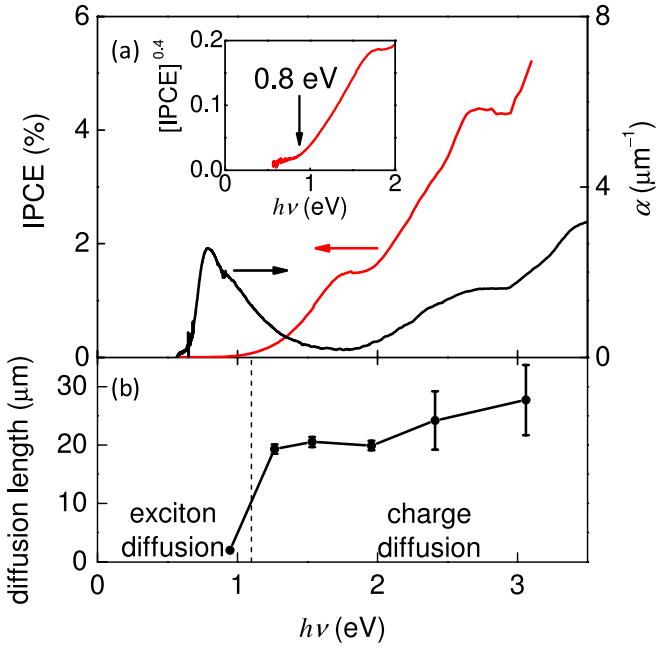

FIG. 3 (color online). (a) Absorption spectrum (black line) and IPCE spectrum (red line) measured for the DBTTF-TCNQ MIM-type PV diode under a reverse-bias condition of 2 MV m^{-1}. The inset shows a plot of $(\mathrm{IPCE})^{0.4}$ against $h\nu$ for the IPCE spectrum. (b) The diffusion length obtained from the LBIC profiles (see Fig. 4) as a function of the incident photon energy.

As can be seen, the decay length at 0.9 eV is much shorter than those at higher photon energies. In sharp contrast, the decay length reaches around 20 μm at 1.3 eV and remains almost constant or increases slightly with increasing photon energy; this photon-energy dependence is summarized in Fig. 3. Note that the true value of the decay length at 0.9 eV should be shorter than the spatial resolution limit for this measurement (2 μm). Actually, the decay length at 0.9 eV is almost the same as those observed for fullerene single crystals (as shown in Fig. 4), whose exciton diffusion length is reported to be a few tens of nanometers [1].

From these results, we conclude that the small decay length at 0.9 eV can be ascribed to CT exciton diffusion, whereas the long decay length above 1.3 eV probably originates from diffusion of free electrons and holes. This consideration is consistent with the Onsager-type photon-energy dependence of the IPCE spectrum. Above 1.3 eV, free electrons and holes should be directly generated by photoexcitation in a manner similar to that in inorganic semiconductors; the diffusion length in Si is reported to be a few hundreds of micrometers [24–26]. These features can be ascribed to the inherent characteristics of CT excitons, which can be dissociated by a small excess photon energy. If we assume that the electron (or hole) diffusion length L is 20 μm, the lifetime τ of photocarriers is estimated to be 160 μs from the relationship $L = \sqrt{D\tau}$, where the diffusion constant D is calculated according to Einstein's relationship $D = \mu kT/e$ by using the field-effect mobility μ (1 cm^2 V^{-1} s^{-1}) [17]. The resulting long lifetime may be

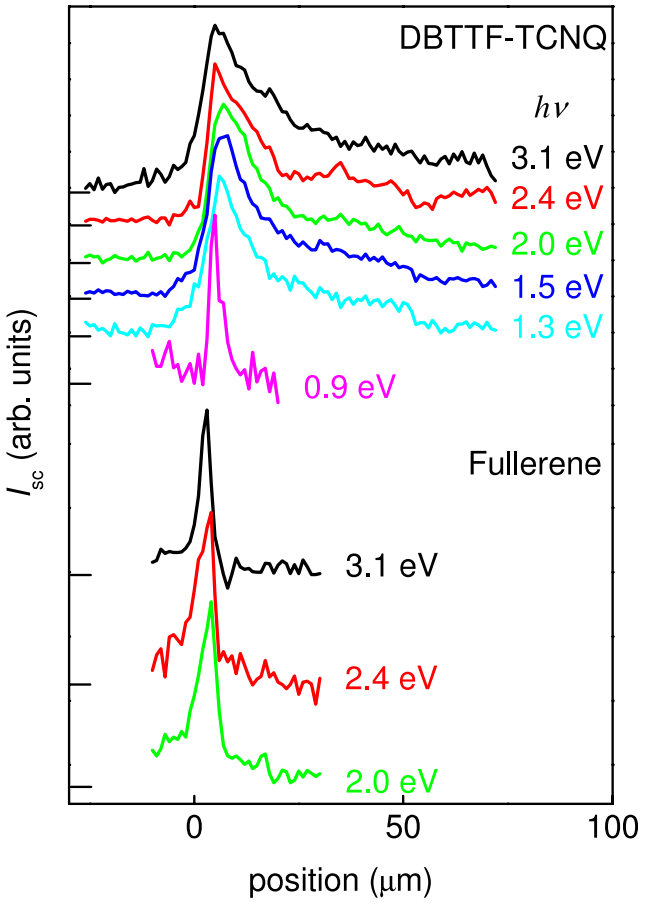

FIG. 4 (color online). LBIC profiles measured at various incident photon energies for DBTTF-TCNQ and fullerene. The results on fullerene were obtained for the single crystal with a size of $0.5 \times 0.5 \times 0.5\ \mathrm{mm}^3$ grown by vacuum sublimation, where we used a pair of gold electrodes for the LBIC measurement.

related to the average time before deep trapping or electron-hole recombination. Also note that the decay length for electrons and holes should be almost the same, as shown in Fig. 1(d), implying that the recombination mechanism may dominate in DBTTF-TCNQ single crystals.

In summary, we have investigated the interfacial charge-dissociation and fundamental PV characteristics of molecular donor-acceptor CT complex single crystals of DBTTF-TCNQ with a narrow energy gap of 0.7 eV. The positive and negative signs of the observed LBIC response allowed us to discriminate between hole and electron photocurrent conductions through the metal–semiconductor interfaces in the single crystals. In a further step, we successfully fabricated a MIM-type PV diode. A photocurrent response was observed above a photon energy of 0.8 eV, around which the diffusion and interfacial dissociation characteristic of CT excitons were observed. We also observed an exceptionally long diffusion length in the LBIC photocurrent profiles; this length was as much as 20 μm at an excitation photon energy of above 1.3 eV, which can be ascribed to direct generation of photocarriers. This readiness to undergo CT exciton dissociation and the long diffusion characteristics of electrons and holes should be advantageous in efficient photodetection or infrared photoelectric conversion in OPCs.

We are grateful to Dr. Michio Kondo (Research Center for Photovoltaics, AIST) for fruitful discussions and to Dr. Yukihiro Takahashi (Hokkaido University) for his help in growing the excellent single crystals. This work was supported by the New Energy and Industrial Technology Development Organization (NEDO) through its Innovative Solar Cell program and also by the Japan Society for the Promotion of Science (JSPS) through its Funding Program for World-Leading Innovative R&D on Science and Technology (FIRST Program).

*To whom all correspondence should be addressed.
t-hasegawa@aist.go.jp

[1] P. Peumans, A. Yakimov, and S. R. Forrest, J. Appl. Phys. **93**, 3693 (2003).
[2] I. G. Hill *et al.*, Chem. Phys. Lett. **327**, 181 (2000).
[3] M. Knupfer, H. Peisert, and T. Schwieger, Phys. Rev. B **65**, 033204 (2001).
[4] B. A. Gregg and M. C. Hanna, J. Appl. Phys. **93**, 3605 (2003).
[5] N. S. Sariciftci, *Primary Photoexcitations in Conjugated Polymers: Molecular Exciton versus Smiconductor Band Model* (World Scientific, Singapore, 1997).
[6] B. R. Rand *et al.*, Prog. Photovoltaics **15**, 659 (2007).
[7] B. P. Rand, D. P. Burk, and S. R. Forrest, Phys. Rev. B **75**, 115327 (2007).
[8] P. Heremans, D. Cheyns, and B. R. Rand, Acc. Chem. Res. **42**, 1740 (2009).
[9] F. Padinger, R. Rittberger, and N. S. Sariciftci, Adv. Funct. Mater. **13**, 85 (2003).
[10] C. Yang *et al.*, J. Am. Chem. Soc. **130**, 16 524 (2008).
[11] J.-S. Kim *et al.*, J. Am. Chem. Soc. **130**, 13 120 (2008).
[12] Y. Zhu, R. D. Champion, and S. A. Jenekhe, Macromolecules **39**, 8712 (2006).
[13] Y. Li and Y. Zou, Adv. Mater. **20**, 2952 (2008).
[14] S. Roquet *et al.*, J. Am. Chem. Soc. **128**, 3459 (2006).
[15] M. Pope and C. E. Swenberg, *Electronic Processes in Organic Crystals* (Oxford University Press, New York, 1982).
[16] J. B. Torrance *et al.*, Phys. Rev. Lett. **46**, 253 (1981).
[17] Y. Takahashi *et al.*, Appl. Phys. Lett. **86**, 063504 (2005).
[18] H. Kobayashi and J. Nakayama, Bull. Chem. Soc. Jpn. **54**, 2408 (1981).
[19] Ch. Kloc *et al.*, J. Cryst. Growth **182**, 416 (1997).
[20] D. A. Redfern *et al.*, J. Electron. Mater. **30**, 696 (2001).
[21] B. Moralejo *et al.*, J. Electron. Mater. **39**, 663 (2010).
[22] Y. Takahashi *et al.*, Appl. Phys. Lett. **88**, 073504 (2006).
[23] E. Silinsh and V. Čápek, *Organic Molecular Crystals: Interaction, Localization, and Transport Phenomena* (American Institute of Physics, New York, 1997).
[24] V. K. S. Ong, J. C. H. Phang, and D. S. H. Chan, Solid State Electron. **37**, 1 (1994).
[25] A. Mandelis *et al.*, J. Appl. Phys. **98**, 123518 (2005).
[26] A. Melnikov *et al.*, J. Appl. Phys. **107**, 114513 (2010).